Chemical Engineering Science 66 (2011) 2745–2757

Contents lists available at ScienceDirect

Chemical Engineering Science

journal homepage: www.elsevier.com/locate/ces

Modeling of turbulent gas–liquid bubbly flows using stochastic Lagrangian model and lattice-Boltzmann scheme

R. Sungkorn [a], J.J. Derksen [b], J.G. Khinast [a,*]

[a] Institute for Process and Particle Engineering, Graz University of Technology, Inffeldgasse 21a, A-8010 Graz, Austria
[b] Chemical and Materials Engineering, University of Alberta, Edmonton, Alberta, Canada T6G 2G6

ARTICLE INFO

Article history:
Received 28 June 2010
Received in revised form
14 March 2011
Accepted 15 March 2011
Available online 21 March 2011

Keywords:
Computational fluid dynamics (CFD)
Multiphase flow
Lattice-Boltzmann
Bubbly flow
Large-eddy simulation
Euler-Lagrange approach

ABSTRACT

In this paper we present detailed, three-dimensional and time-resolved simulations of turbulent gas–liquid bubbly flows. The continuous phase is modeled using a lattice-Boltzmann (LB) scheme. The scheme solves the large-scale motions of the turbulent flow using the filtered conservation equations, where the Smagorinsky model has been used to account for the effects of the sub-filter scales. A Lagrangian approach has been used for the dispersed, bubbly phase. That is we update the equations of motion of individual bubbles. It is shown that the incorporation of the sub-filter scale fluid fluctuations along the bubble trajectory improves the predictions. Collisions between bubbles are described by the stochastic inter-particle collision model based on kinetic theory developed by Sommerfeld (2001). It has been found that the collision model not only dramatically decreases computing time compared to the direct collision method, but also provides an excellent computational efficiency on parallel platforms. Furthermore, it was found that the presented modeling technique provides very good agreement with experimental data for mean and fluctuating velocity components.

1. Introduction

Many processes in the chemical and pharmaceutical industry involve turbulent gas–liquid flows. The phenomena encountered in these processes are highly complex, such as those in bubble column reactors (Joshi, 2001; Ranade, 2002). In a bubble column reactor, the flow patterns are generated not only by the interactions between the phases on a macroscopic scale, but also relate to small scale flows such as the wakes behind individual rising gas bubbles. The various scales interact and create complex, turbulent flow. It exhibits unsteady (time-dependent), three-dimensional turbulent behavior characterized by a wide range of time and length scales, from small vortices shed by bubbles to macroscopic circulation patterns with the size of the reactor. These flow patterns relate to the operating and design variables. Therefore, a descriptive engineering model which provides thorough understanding of the hydrodynamics in gas–liquid bubbly flows is essential for analyzing, optimizing, designing and scaling-up of these processes.

Over the past decades, computational fluid dynamics (CFD) have been adopted by large numbers of researchers to study the underlying physics of turbulent gas–liquid bubbly flows. Accordingly, enormous efforts have been directed at establishing a framework for modeling multiphase flows, including the development of closures for inter-phase forces. Using the "hierarchy-of-models" concept introduced by Delnoij (2001), three levels of modeling can be identified based on the spatial and temporal resolution of the model. At the finest level, where relevant scales include individual bubbles, small-scale vortices behind bubbles and bubble–bubble interactions, the volume-of-fluid (VOF) approach of Hirt and Nichols (1981) or the front tracking (FT) approach of Unverdi and Tryggvason (1992) may be employed. However, these approaches are restricted to a single bubble or a few interacting bubbles due to the extensive computational requirements (Deen et al., 2004). At the intermediate level each individual bubble or a parcel of bubbles is represented by a single point, and its trajectory is tracked by solving its equation of motion. This approach is known as the Euler–Lagrange (EL) approach. In contrast to the VOF and FT approach, the EL approach requires closure relations to account for the inter-phase forces, which can be obtained from empirical relations or from simulations with a more sophisticated level of resolution (i.e., VOF or FT). Nevertheless, the EL approach is highly flexible with respect to incorporating microscopic and bubble-level phenomena, such as bubble–bubble interactions, coalescence or break-up of bubbles (Ranade, 2002; Van den Hengel et al., 2005). Due to the significant computational resources required, the EL approach becomes infeasible for simulations of large industrial-scale bubble columns or stirred tanks, which may contain tens of millions of bubbles. For such cases, the coarsest level of modeling,

* Corresponding author. Tel.: +43 316 873 7464; fax: +43 316 873 7963.
E-mail address: khinast@tugraz.at (J.G. Khinast).

0009-2509/$ - see front matter © 2011 Elsevier Ltd. All rights reserved.
doi:10.1016/j.ces.2011.03.032

Table 1
Expressions for the forces acting on a bubble.

Force	Closure
$\mathbf{F}_G=(\rho_p-\rho_l)V_p\mathbf{g}$	–
$\mathbf{F}_S=\rho_l V_p D_t\mathbf{u}$	–
$\mathbf{F}_D=-\frac{1}{2}C_D\rho_l\pi r_p^2\lvert\mathbf{u}_p-\mathbf{u}\rvert(\mathbf{u}_p-\mathbf{u})$	$C_D=\max\left[\min\left[\frac{24}{Re_p}(1+0.15\mathrm{Re}_p^{0.687}),\frac{48}{Re_p}\right],\frac{8}{3}\frac{Eo}{Eo+4}\right]$
$\mathbf{F}_L=-C_L\rho_l V_p(\mathbf{u}_p-\mathbf{u})\times\nabla\times\mathbf{u}$	$C_L=\begin{cases}\min[0.288\tanh(0.121Re_p),f(Eo_d)], & Eo_d<4\\ f(Eo_d), & 4<Eo_d\le 10\\ -0.29, & Eo_d>10\end{cases}$
	$Eo_d=\frac{Eo}{E^{2/3}},\ E=\frac{1}{1+0.163Eo^{0.757}}$
	$f(Eo_d)=0.00105Eo_d^3-0.0159Eo_d^2-0.0204Eo_d+0.474$
$\mathbf{F}_A=-C_A\rho_l V_p(D_t\mathbf{u}_p-D_t\mathbf{u})$	$C_A=0.5$

i.e., the Euler–Euler (EE) approach (also called two-fluid model), which treats both phases as interacting continua, is applied. Despite its lack of detail at the bubble-level, it has been widely used in the past decade for the engineering modeling of large-scale industrial bubble column reactors due to the relatively limited computational resources needed. However, a detailed understanding of multiscale phenomena, including large-scale mixing patterns, as well as breakup and coalescence of bubbles, is crucial for analyzing, designing and scaling of processes, especially for processes that are critical in terms of mass transfer and chemical reactions. As may be clear from the above, limitations of the currently available modeling techniques and computational resources makes resolution of bubbly flow hydrodynamics down to the bubble-scale not practical.

The goal of this study is to introduce a novel approach which allows the modeling of turbulent gas–liquid bubbly flows using the EL approach to obtain detailed information of the hydrodynamics down to the bubble-scale with only moderate computational resource requirements. The proposed approach provides an alternative to obtain insights into large-scale processes. However, for the validation purpose, simulations of a lab-scale system have been carried out and presented here. The modeling technique used in this study includes the following elements:

- The continuous liquid phase is modeled using a variation of the lattice-Boltzmann (LB) scheme due to Somers (1993) and Eggels and Somers (1995). We use the scheme to solve for the large-scale motions of the turbulent flow using the filtered conservation equations, where the Smagorinsky subgrid-scale model (Smagorinsky, 1963) has been used to model the effects of the sub-filter scales. It has been demonstrated that the LB scheme can accurately represent turbulent flow hydrodynamics, including single-phase flows (Derksen and Van den Akker, 1999), as well as multiphase flows (Derksen et al., 2008; Derksen, 2003, 2010). Due to the locality of operations, lattice-Boltzmann schemes have high computational efficiency, especially on parallel platforms (Derksen and Van den Akker, 1999).
- For the dispersed gas phase, the trajectories of the individual bubbles are computed in the Lagrangian manner taking into account the sum of net gravity force, forces due to stress gradients, drag force, lift and added mass forces. The force coupling between the fluid phase and the bubbles, i.e., the two-way coupling between the phases, is achieved by the "cheap clipped fourth-order polynomial mapping function" introduced by Deen et al. (2004). A set of closure relations for these inter-phase forces were carefully chosen from literature data (Hu, 2005; Joshi, 2001; Loth, 2000), see Table 1. It should be noted that the EL approach does not resolve the gas–liquid interface and the size of the bubbles considered in this work is smaller than the grid-spacing. The impact of turbulence on the bubbles, i.e., the fluctuations of the sub-filter or residual fluid velocity along the bubble trajectory, is computed using the Langevin equation model introduced by Sommerfeld et al. (1993). Collisions of bubbles are governed by the so-called stochastic inter-particle collision model of Sommerfeld (2001). Although the model was originally proposed for solid particle-laden flows, it has also been successfully applied to modeling of bubbly flow (Sommerfeld et al., 2003).

Although various elements of this approach have been reported in the literature, the presented EL model, for the first time assesses the feasibility of using the LB scheme with the stochastic particle model to obtain a fast, yet detailed understanding of turbulent bubbly flows. Thus, the combination of these two techniques constitutes a novel development in the simulation of bubbly multiphase flows.

This paper is organized in the following manner: in the next section, the modeling approach for turbulent bubbly flows in the EL framework will be discussed in more detail. In the subsequent section, the model validation, including the impact of the modeling techniques and choices on the predicted results, will be presented. The computational performance of the presented modeling technique will be discussed as well, followed by a summary and conclusions.

2. Modeling of gas–liquid bubbly flows

2.1. Liquid phase hydrodynamics

In our work the lattice-Boltzmann (LB) method is used for modeling the continuous liquid phase. The LB method is based on a simple form of the Boltzmann kinetic equation, which can be used to recover the macroscopic hydrodynamic behavior of fluids (Bernaschi et al., 2010). The specific LB scheme employed here is due to Somers (1993) (see also Eggels and Somers, 1995; Derksen and Van den Akker, 1999). It provides a second-order discretization in space and time for the incompressible Navier–Stokes equations on a uniform, cubic lattice. This scheme was chosen because of its robustness for turbulence simulations and its inherently high parallelization efficiency. The robustness results from its explicit treatment of the higher-order terms leading to enhanced stability at low viscosities. This allows us to reach relatively low viscosities and thus high Reynolds numbers and makes the scheme suitable for turbulence simulations (Derksen, 2010). The inherent parallelism of the LB method is due to the locality of its arithmetic operations. Thus, the communication

between processors requires only limited amounts of overlapped-boundary data, resulting in an efficient parallel structure.

In this paper, we limit ourselves to a flow configuration in which the motion of the continuous liquid phase is solely driven by the dispersed gas bubbles. Bubble collisions are expected to have a significant effect on the hydrodynamics. However, coalescence and breakup of bubbles are neglected in the present study as we consider a dilute system. In this flow, the turbulent stress can be divided into two components, i.e., one component due to bubble buoyancy leading to liquid velocities above the turbulence onset, and one component due to the so-called pseudo-turbulence, caused by the fluctuations of the bubbles (i.e., the motion of bubbles relative to the liquid which results in turbulent-like flows) (Hu and Celik, 2008).

A filtering process with a filter width equal to the grid space was applied to the conservation equations of the liquid phase to resolve only the evolution of the large-scale motions. The resolved flow can be interpreted as a low-pass filtered representation of the real flow. The impact of the residual motion that resides at scales smaller than the filter width, i.e., the subgrid-scale (SGS), is modeled using the Smagorinsky SGS model (Smagorinsky, 1963). In the Smagorinsky model, the SGS motion is considered to be purely diffusive, and the model only drains energy from the resolved motions without feed-back. For finer grid spacing, a larger fraction of the eddies and more of the energy contained in the flow field are resolved. However, the choice of the grid spacing in the present work is also restricted by the requirements of the EL approach, i.e., the point-volume assumption that the interfacial details are not resolved. Therefore, the grid spacing should be larger than the (physical) bubble diameter. In the case where the bubble diameter is larger than the grid spacing, the bubble's interfacial detail becomes important and should be resolved (Nicěno et al., 2009). This is also consistent with the grid size considerations discussed in the work of Milelli et al. (2001). Based on considerations of the energy spectra and modeling closures for the inter-phase forces, they stated that the grid space should be at least 50% larger than the bubble diameter, i.e., the ratio between the grid spacing h and the bubble diameter d_p should be larger than 1.5.

In the present paper, the ratio between h and d_p was chosen to be 1.25, similar to that in the work of Nicěno et al. (2009), and clearly smaller than the criterion proposed by Milelli et al. (2001). However, it can be argued that it is known *a priori* that the flow pattern of the bubble column is dominated by a bubble plume, which meanders from one side of the bubble column to the other side. Therefore, it can be concluded that the largest scale, which contains most energy, will be of the size of the domain cross-section (Nicěno et al., 2009). The grid resolution employed here is a compromise between sufficiently fine to capture the most energetic eddies, and sufficiently coarse to stay close to the Milelli criterion (Milelli et al., 2001).

The SGS model used in the present work is the Smagorinsky model adopted directly from the single-phase SGS model. In this model, the eddy viscosity v_t concept is used to represent the impact of the SGS motion as

$$v_t = (C_S \Delta)^2 \sqrt{S^2}, \tag{1}$$

with the Smagorinsky constant C_S, the filter width Δ (with size equal to the grid spacing h) and the resolved deformation rate $\sqrt{S^2}$. As pointed out in the work of Hu and Celik (2008) the so-called pseudo (or bubble-induced) turbulence possesses a universal energy spectrum with identifiable power-law decay. This, however, is different from the classical $-5/3$ decay. Therefore, the residual motion arising from both turbulence and pseudo-turbulence could (in principle) be captured using a dedicated subgrid-scale model acting on the continuous phase. However, such a (reliable and accurate) SGS model for multiphase flows is not readily available (Hu, 2005), so that we reverted to the use of the Smagorinsky model for our simulations of gas–liquid flows, justified by favorable results as will be shown later in this paper.

Since the simulations discussed here are restricted to the dilute dispersion condition (global gas void fraction up to 2%), we assume that the void fraction term in the conservation equations for the continuous phase only has a relatively small effect on the flow field, and can be neglected. Therefore, the filtered conservation equations (equipped with momentum source terms representing the bubbles) for single-phase flows are approximately valid. This assumption has been tested successfully by some researchers, e.g., Hu and Celik (2008) and Hu (2005), for a relatively dilute void fraction gas–liquid bubbly flow (up to 1%) and Derksen (2003) for dilute suspensions (solid volume-fractions up to 3.6%).

In the present paper, the forces imposed by a bubble on the continuous phase and vise versa (i.e., two-way coupling) are considered. These local interactions are represented via the inter-phase force terms in the conservation equations, i.e., the drag force $\mathbf{F}_D$, lift force $\mathbf{F}_L$ and added mass force $\mathbf{F}_A$. Expressions for these forces are discussed in the following section.

2.2. Bubble dynamics

Each individual bubble is treated as a single, point-volume particle/bubble with constant mass and has three degrees of freedom associated to it, i.e., three spatial coordinates. Its trajectory is tracked based on Newton's equation of motion

$$d_t x_p = \mathbf{u}_p, \tag{2}$$

$$\rho_p V_p d_t \mathbf{u}_p = \mathbf{F}_p, \tag{3}$$

where x_p, $\mathbf{u}_p$, ρ_p, V_p and $\mathbf{F}_p$ represent the center position of the bubble, the velocity, the bubble density, the bubble volume and the net force, respectively. Here, the net force $\mathbf{F}_p$ acting on each individual bubble is the sum of net gravity force $\mathbf{F}_G$, forces due to stress gradients $\mathbf{F}_S$, drag force $\mathbf{F}_D$, net transverse lift force $\mathbf{F}_L$ (i.e., the sum of shear- and wake-induced lift forces), added mass force $\mathbf{F}_A$ and Basset history force $\mathbf{F}_H$

$$\mathbf{F}_p = \mathbf{F}_G + \mathbf{F}_S + \mathbf{F}_D + \mathbf{F}_L + \mathbf{F}_A + \mathbf{F}_H. \tag{4}$$

It has been reported by Loth (2000) that the Basset history force is negligible when time-averaged or when integral quantities in a turbulent fluid velocity field are of interest. Thus, the Basset history force is neglected in this work. Formulations of the forces acting on a bubble have been discussed in detail by a number of researchers, see for example, Loth (2000), Joshi (2001) and Hu (2005). With the expressions summarized in Table 1 and substituting Eq. (4) into (3), the following set of equations is solved in order to keep track of individual bubbles:

$$\rho_p V_p d_t \mathbf{u}_p = (\rho_p - \rho_l) V_p \mathbf{g} + \rho_l V_p D_t \mathbf{u} - \frac{1}{8} C_D \rho_l \pi d_p^2 |\mathbf{u}_p - \mathbf{u}| (\mathbf{u}_p - \mathbf{u}) - C_L \rho_l V_p (\mathbf{u}_p - \mathbf{u}) \times \nabla \times \mathbf{u} - C_A \rho_l V_p (D_t \mathbf{u}_p - D_t \mathbf{u}), \tag{5}$$

with ρ_l being the liquid phase density, $\mathbf{u}$ the liquid velocity, and C_D, C_L and C_A the drag, lift and added mass force coefficients, respectively. The drag and lift coefficients depend on the bubble Reynolds number $Re_p = |\mathbf{u}_p - \mathbf{u}| d_p / v_l$ and the Eötvös number $\mathrm{Eo} = (\rho_l - \rho_p) |\mathbf{g}| d_p^2 / \sigma$. It should be noted that the drag coefficient does not have a local void-fraction dependency because the gas volume-fractions considered here are sufficiently low not to include a dependency of the drag coefficient on the local void-fraction. Similar considerations apply to the buoyancy term.

The liquid velocity at the bubble position $\mathbf{u}$ introduced in Eq. (5) is composed of the resolved liquid velocity and a (residual) liquid fluctuating component $\mathbf{u}'$. The latter component is recovered using the so-called Langevin equation model introduced by Sommerfeld et al. (1993). In this model, a correlation function $R_p(\Delta t,\Delta r)$ (see Appendix) is used to correlate the fluctuation velocity from the old to the new bubble location:

$$\mathbf{u}'_{n+1} = R_p(\Delta t,\Delta r)\mathbf{u}'_n + \sigma_{SGS}\sqrt{1-R_p(\Delta t,\Delta r)}\,\xi, \tag{6}$$

where σ_{SGS} is the characteristic residual motion, and ξ a Gaussian random number with a mean value of zero and a standard deviation of one. Based on the assumption that the residual turbulent motion is locally homogeneous and isotropic, the characteristic residual motion was estimated by $\sigma_{SGS} = \sqrt{2/3k_{SGS}}$. The SGS kinetic energy k_{SGS} was approximated based analysis of the energy spectrum as (Pozorski and Apte, 2009)

$$k_{SGS} = \left(\frac{v_t}{0.067\Delta}\right)^2. \tag{7}$$

The interpolation of the liquid properties on the Eulerian grid to the bubble centroid on the Lagrangian reference frame is achieved using a mapping function ς described by the so-called cheap clipped fourth-order polynomial proposed by Deen et al. (2004)

$$\varsigma(x-x_p) = \frac{15}{16}\left[\frac{(x-x_p)^4}{n^5} - 2\frac{(x-x_p)^2}{n^3} + \frac{1}{n}\right] \text{ with } |x-x_p| \le n, \tag{8}$$

where x is the position of a neighboring grid node, and n is half of the predefined influence diameter (set to $2d_p$ in this work). With this mapping function, a property, such as the liquid velocity at the bubble centroid $\mathbf{u}(x_p)$, is evaluated by the integration of the liquid velocity at the neighboring grid nodes (that is located inside the influence diameter) $\mathbf{u}(x)$. The forces exerted on the continuous phase by the bubbles are treated as a point force and distributed to the continuous phase using a similar mapping function. A further discussion concerning mapping techniques can be found in the work of Deen et al. (2004) and Hu and Celik (2008).

For turbulent bubbly flow simulations, numerical instabilities can be induced by many factors, for instance, the evolution of bubbles with a very small mass, and/or strong fluctuations generated by forces exerted from the bubbles on the liquid. In order to avoid these instabilities, we used a very small time step to maintain the velocity update due to the inter-phase force (in lattice units) within the compressible limit of the LB scheme. We under-relax the distributed force with a relaxation factor of 0.25. Additionally, the mapping technique with the influence diameter concept discussed above also helps to prevent high concentration of forces exerted by a bubble.

2.3. Stochastic inter-particle collision model

Collisions between bubbles are considered using the stochastic inter-particle collision model introduced by Sommerfeld (2001). Instead of direct collision calculation, where a large amount of information from surrounding bubbles is required, only a fictitious collision partner and a collision probability according to kinetic theory are generated for each bubble at each time step of the trajectory calculation. In this model, the size and the velocity of the fictitious collision partner is sampled from the local distribution functions stored at each grid node. Since the bubble size used is relatively large, in order to obtain representative properties, the distribution functions is computed from a set of nodes that reside in the influence diameter of the bubble using a similar mapping technique as in the previous section. Hence, in this work, the so generated fictitious bubble can be considered as representative for the bubbles in its direct vicinity.

The velocity components of the fictitious bubble consist of the local mean velocity $\mathbf{u}_{fict}$ and the fluctuating component $\mathbf{u}'_{fict}$ which also compose of three degrees of freedom. The first component is obtained from the method discussed above. The latter component is obtained via a correlation proposed by Sommerfeld (2001).

$$\mathbf{u}'_{fict} = R(St)\mathbf{u}'_{real} + \boldsymbol{\sigma}_p\sqrt{1-R(St)^2}\,\xi, \tag{9}$$

with $\mathbf{u}'_{real}$ being the fluctuating velocity components of the real bubble which are evaluated based on the ensemble-averaged bubble velocity and the instantaneous bubble velocity. $R(St)$ is the correlation function based on the bubble Stokes number St, and $\boldsymbol{\sigma}_p$ is the local rms value of the bubble velocity components. The bubble Stokes number St is defined as the ratio of bubble response time τ_p and the Lagrangian integral time scale T_L, as suggested by Ho (2004) (see Appendix). As can be seen in Eq. (9), the degree to which the bubble fluctuating velocities are correlated depends on their response to turbulent fluctuations, which is characterized by the Stokes number. Based on the calculations obtained from large eddy simulations, Sommerfeld (2001) reports the dependence of the correlation function on the Stokes number as

$$R(St) = \exp(-0.55St^{0.4}). \tag{10}$$

The occurrence of a collision is determined by the collision probability P_{coll} given by kinetic theory

$$P_{coll} = \frac{\pi}{4}(d_{p,i}+d_{p,j})^2\,|\mathbf{u}_{p,i}-\mathbf{u}_{p,j}|\,n_p\Delta t, \tag{11}$$

where $d_{p,i}$ and $d_{p,j}$ are the bubble diameters, $|\mathbf{u}_{p,i}-\mathbf{u}_{p,j}|$ the instantaneous relative velocity between the considered and the fictitious bubble, and n_p the number of bubbles per unit volume in the respective grid nodes. A collision takes place when a random number RN, generated by a uniform distribution in the interval [0,1], becomes smaller than the collision probability, i.e., $RN < P_{coll}$. The technique we have employed for the generation of the random number follows the algorithm presented in the work of Press et al. (1992). In the case of a collision, the point of impact on the bubble surface is statistically determined based on a collision cylinder (see Sommerfeld (2001) and Ho (2004) for a detailed description). In this work, the bubble–bubble collisions are assumed to be fully elastic.

2.4. Parallelization aspects

As mentioned previously, the lattice-Boltzmann (LB) scheme has an inherently high parallelization potential due to its locality of operations, e.g., data required for updating the flow in a grid point are obtained from its neighbors, and the stress tensor is explicitly obtained from the data stored in a single node. In the present implementation, parallelization of the continuous phase is achieved by axially dividing the computational domain into subdomains. In contrast to the conventional parallelization strategy used in single-phase LB schemes where only boundary values are communicated, the present multiphase (EL) numerical scheme requires the communication of a number of grid layers, depending on the bubble diameter and the influence diameter. For instance, a bubble with a diameter of $0.8h$ and an influence diameter of $2d_p$ located near the boundary between subdomains would require data not only from the nodes at the boundary but also from the other three rows behind the boundary for the distribution and redistribution of properties between the bubble and the liquid phase (see Fig. 1). It should be noted that although information from two rows behind the boundary is used in the mapping function, one additional row (the third row) is required for the evaluation of the curl of the fluid velocity $\nabla\times\mathbf{u}$. It will be

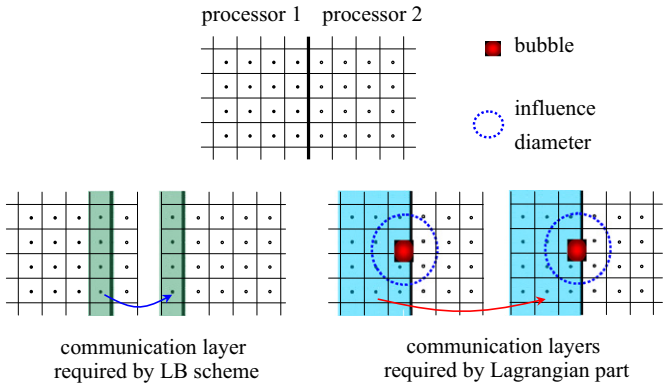

Fig. 1. Parallelization strategy (left) single communication layer required by the LB scheme and (right) three communication layers required by the Lagrangian part.

shown in the next section that despite the larger amount of data being communicated between the subdomains, the speedup for the continuous phase calculation is still excellent.

Generally, the parallelization of the dispersed phase is significantly more complicated than that of the continuous phase. The first complication is due to the handling of bubble–bubble collisions in the vicinity of subdomain borders. For direct collisions handling, large amounts of information of bubbles crossing borders as well as bubbles close to the border need to be communicated. This is overcome by employing the stochastic inter-particle collision model described above. Since the model requires only information stored at the Eulerian grid nodes, only a limited amount of information concerning bubbles crossing borders is communicated. Another complication arises from the dynamical nature of bubbles, which makes their spatial distribution non-uniform. In order to achieve high parallel performance, a load-balancing strategy needs to be considered. In our case, unbalanced loading occurred only at the initial stages of the simulation. After the onset of aeration, the loading at each processor was approximately balanced. Hence, a static domain decomposition is considered efficient enough for the parallelization of the dispersed phase.

2.5. The Deen bubble column experiment

In the present study, the bubble column experiment performed by Deen et al. (2001), hereafter called the Deen case, was used as a reference for validating the simulations. Their three-dimensional rectangular bubble column has a width, depth and height of 0.15, 0.15 and 0.45 m, respectively. Air bubbles were introduced at the bottom-center plane with an area of 0.03×0.03 m^2 and a superficial gas velocity of 4.9 mm/s. A bubble mean diameter in the order of 4 mm was observed in their experiments using digital image analysis. It was assumed to have that uniform size with spherical shape in the simulations presented in this paper.

2.6. Numerical implementation

In all the following simulations, the fluid domain is discretized by a uniform cubic grids of $30 \times 30 \times 90$ lattices in width, depth and height, respectively. This results in a bubble size of 0.8 times the lattice distance. An influence diameter is set to $2d_p$. The criteria for the selection of the grid spacing have been described previously. A no-slip, i.e., a bounce-back, boundary condition is applied at every sides of the computational domain except for the top where a free-slip boundary condition is applied. Bubbles are injected at the bottom of the column through 49 inlet positions. Once a bubble (with its physical surface) touches the top surface of the column, it will be discarded from the simulation. From our simulations, it has been observed that a maximum number of 7000 bubbles were tracked. The calculation starts with the quiescent liquid and proceeds with a time step for the liquid phase of 10 μs for 150 s. The time step used in this work has the same order of magnitude as used for the solid suspension simulation in a stirred tank by Derksen (2003). Using 8 processors, the simulation time (i.e., the real clock time) is approximately 100 h for case numbers 0–3. A sub-time step of 1 μs is used for the calculation of the dispersed gas phase. The reason for this small time step used in this work is to obtain stability of the LB scheme as well as Newton's equation of motion (Eq. (5)).

3. Results and discussion

In this study the gas–liquid flow from the Deen case is simulated using the modeling technique described in the previous sections. The gas–liquid flow hydrodynamics of the Deen case will be discussed first, followed by a study of the sensitivity of the SGS fluctuations, as well as the Smagorinsky constant C_S. The parallelization performance of our code will also be assessed. Six different cases were considered and Table 2 summarizes the characteristics of these simulations.

3.1. Two-phase flow

A series of snapshots of the evolving bubble plume for the standard case (case 0) are shown in Fig. 2(a)–(d). These snapshots are taken at consecutive points in time of 20, 50, 100 and 150 s. As can be seen, the lower part of the plume fluctuates within a small range, while the upper part fluctuates strongly around the bubble column in a random manner. This behavior was also observed in the experiments by Deen (2001) and Deen et al. (2001). The corresponding instantaneous liquid flow fields at the vertical mid-depth plane are shown in Fig. 3(a)–(d). Several large and small vortices can be observed in the liquid phase. These vortices interact with each other and significantly change their size, shape and position randomly with time. The random velocity fluctuation of the liquid phase can be seen clearly in the plot of the velocity at an arbitrary point in the column, as shown in Fig. 4. These results illustrate the strong coupling between the fluctuation of the bubble plume and the turbulent flow field in the liquid phase.

A quantitative comparison of the time-averaged hydrodynamics between predicted results and experimental data is required for the validation of the presented modeling technique. In order to obtain statistically meaningful results, a sufficiently long simulation period has to be considered. Since the fluctuation of the bubble plume was only observed after the onset of aeration, the time-averaged quantities were calculated starting from 20 s. The average liquid velocity and velocity fluctuations at various simulation times are shown in Fig. 5. It can be seen that all

Table 2
Overview of the different simulation cases.

Case	SGS velocity	Collision	C_S	h/d_p
0	Eq. (6)	Eq. (11)	0.10	1.25
1	–	Eq. (11)	0.10	1.25
2	Eq. (6)	Eq. (11)	0.08	1.25
3	Eq. (6)	Eq. (11)	0.12	1.25
4	Eq. (6)	Eq. (11)	0.10	1.50
5	Eq. (6)	Eq. (11)	0.10	1.10

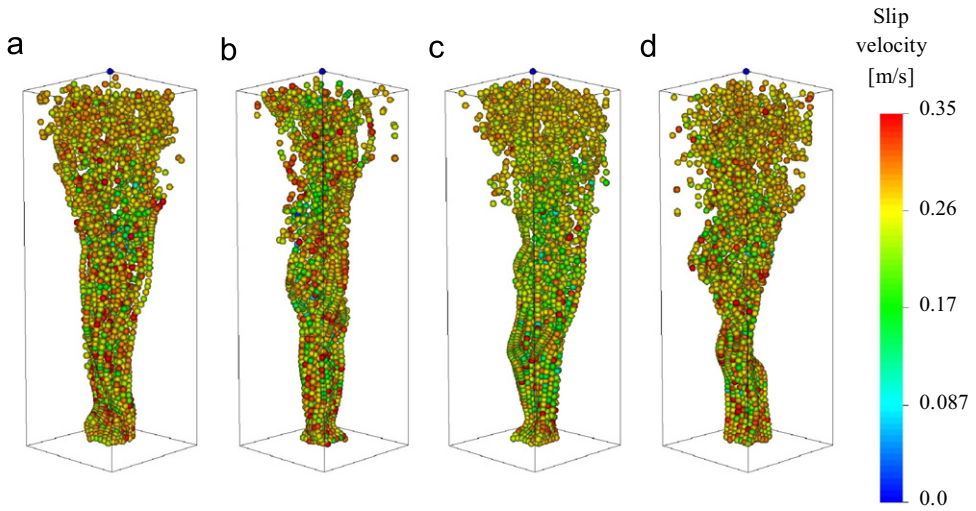

Fig. 2. Snapshots of the bubble dispersion pattern after 20, 50, 100 and 150 s. The bubbles are colored by the magnitude of bubble's slip velocity. Note that the bubbles are magnified for visualization purpose, not to scale. (For interpretation of the references to color in this figure legend, the reader is referred to the web version of this article.)

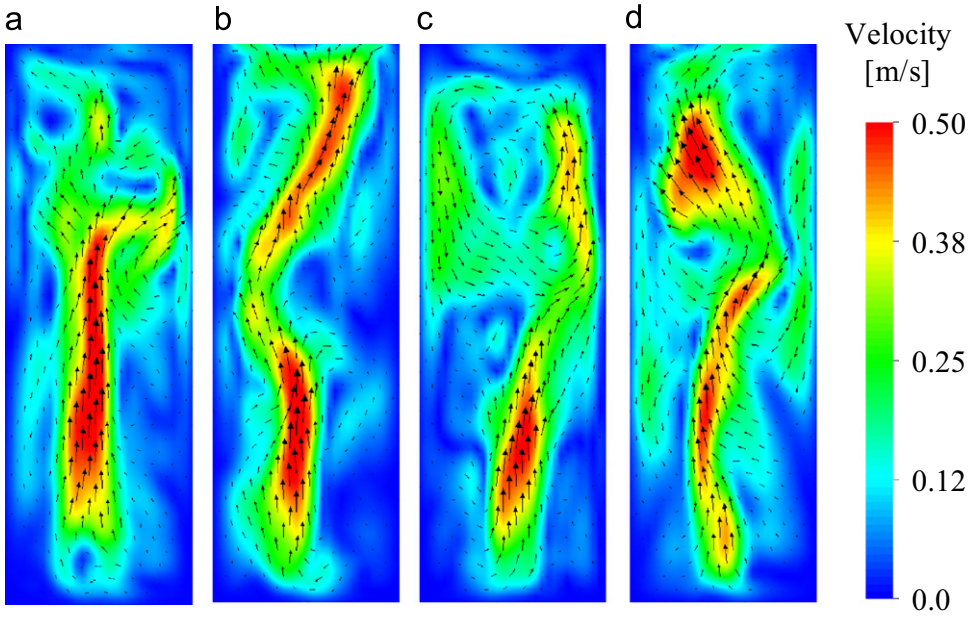

Fig. 3. Snapshots of the liquid phase velocity at the mid-plane after 20, 50, 100 and 150 s.

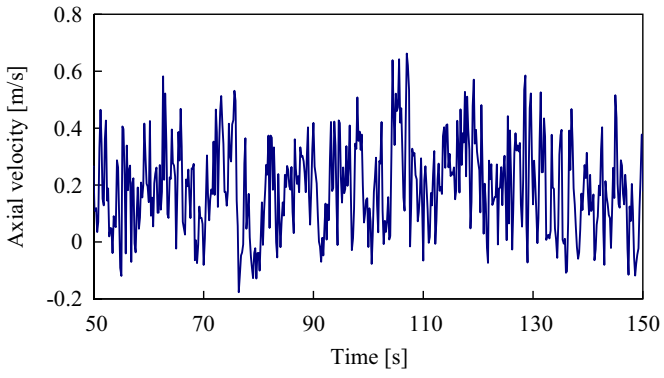

Fig. 4. Axial liquid velocity as a function of time at the center line of the column and a height of 0.28 m.

quantities are converged after the simulation time of approximately 125 s.

A comparison of the predicted mean vertical velocity with experimental data in Fig. 5(a) shows excellent agreement between simulation and experiment. The magnitude and the position of the local maximum are accurately predicted. The overall velocity profile is correctly reproduced quantitatively and qualitatively. Only a small deviation of the velocity near the wall region can be noticed. This might be attributed to an insufficient resolution of the near-wall structures, which may be resolved by introducing a wall function or an adaptive grid refinement at the near-wall region (with some computational expenses). In Fig. 5(b) and (c), the second-order statistics related to the turbulence quantities, i.e., the fluctuating components of the resolved flow field, predicted by the simulations are compared with the experimental data. This comparison is necessary

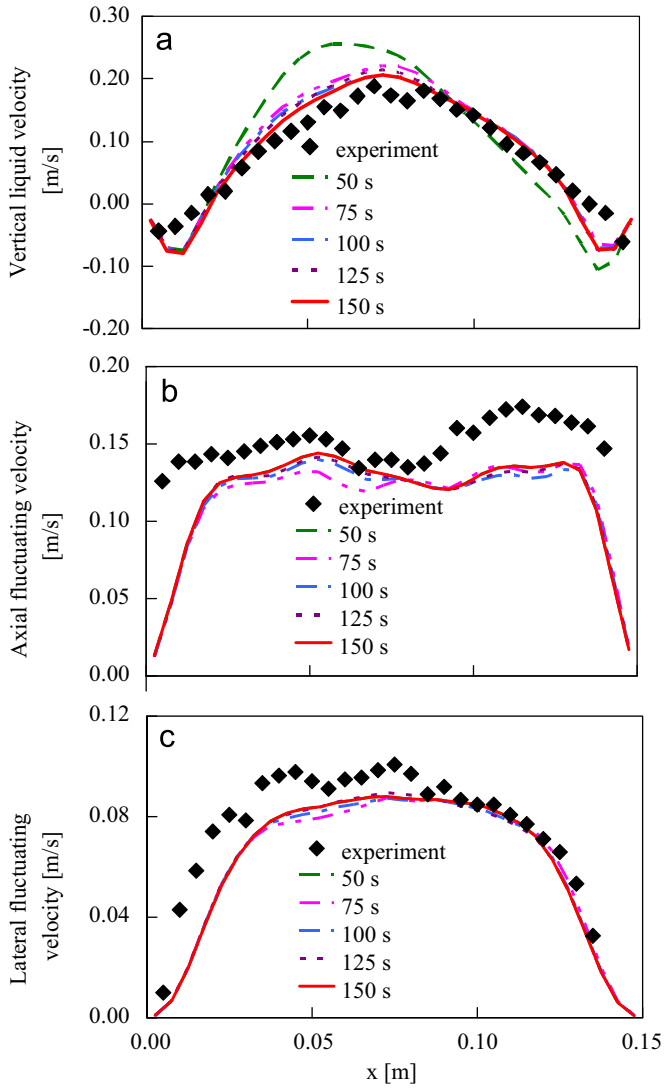

Fig. 5. Comparison of the predicted and experimental liquid velocity and fluctuating velocity components for the standard case (case 0) at a height of 0.28 m and a depth of 0.075 m after different averaging periods.

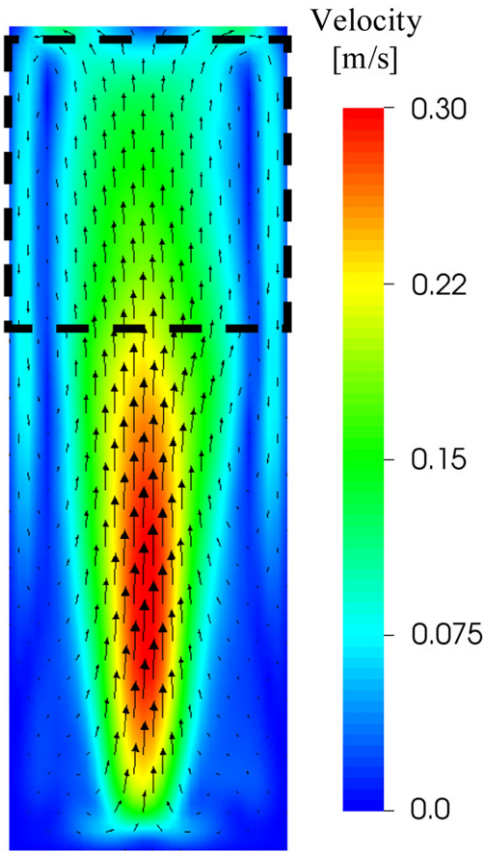

Fig. 6. Long-term average of the liquid velocity field in the mid-depth plane.

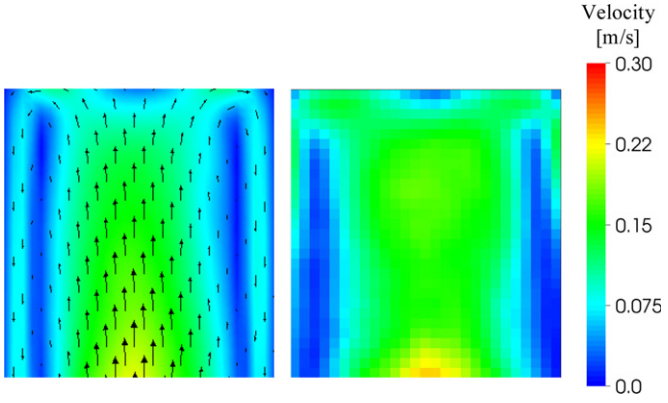

Fig. 7. Predicted and experimental long-term average of the liquid velocity field in the mid-depth plane at the upper part of the bubble column.

to obtain confidence in the prediction of problems involving turbulent flows. The vertical component of the resolved fluctuating liquid velocity is shown in Fig. 5(b). The twin-peaked shape observed in the experiments is correctly reproduced. Quantitatively, the magnitude of the vertical fluctuating component is slightly under-predicted, except at the near-wall regions where larger deviations can be noticed. Fig. 5(c) shows the resolved lateral fluctuating liquid velocity. It should be noted that in order to compare simulation results to the experimental data which are measured in two dimensions, only one horizontal velocity component (on the measured plane) is used throughout this work, unless otherwise stated. Again, the predicted profile agrees very well with the experimental data. Additionally, it is apparent that the fluctuations in the vertical direction are larger than in the lateral direction, which implies that the turbulence is anisotropic.

A long-term average of the liquid flow fields is shown in Fig. 6. The flow is dominated by the upward flow induced by the bubble plume. Two thin circulation zones close to the wall region can be observed over the height of the bubble column. The long-term average of the liquid flow field at the upper part of the column is compared with the experimental data in Fig. 7. The structure of the flow field, i.e., upward flow in the middle and thin circulation zones close to the wall, is correctly reproduced by the simulation. A contour plot of the resolved liquid phase turbulent kinetic energy *TKE* in the mid-plane is given in Fig. 8. Two regions of high turbulent activity (i.e., high *TKE*) separated by the center line of the bubble plume can be observed. It can be further seen that, due to the injection of the bubbles, *TKE* increases from the bottom, and has maximum at about half the height of the column. Consequently, since the top surface dampens the fluctuation of the liquid phase, the *TKE* decreases from the middle to the top of the column. A comparison between the predicted *TKE* at the upper part of the column with the experimental data is shown in Fig. 9. The simulation underpredicts the measured *TKE*. Additionally, the gas void-fraction profiles at different height levels are shown in Fig. 10. To determine the Eulerian gas volume fraction distribution from the Lagrangian simulation, the mapping

function presented in the previous section was used. It can be seen that at the bottom of the column, where the bubble inlet is located, the profile has a high concentration of gas only near the center line of the column, while the profile tends to broaden towards the top of the column.

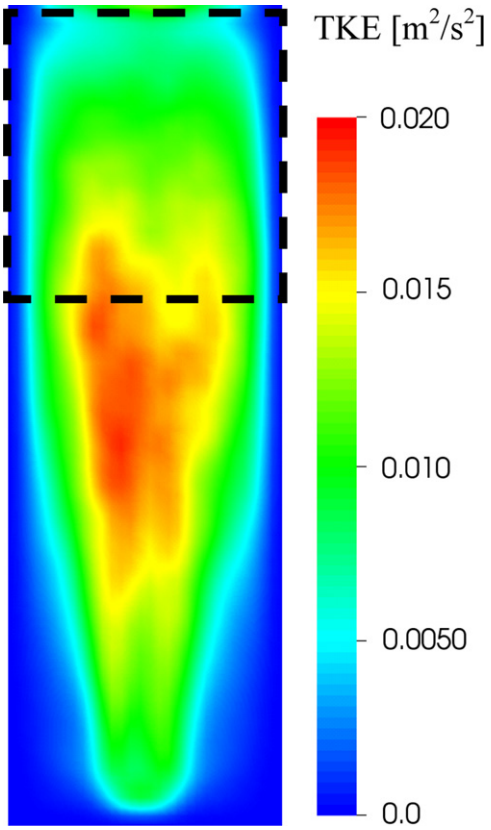

Fig. 8. Long-term average of the turbulent kinetic energy contour in the mid-depth plane.

3.2. Subgrid-scale velocity

The influence of the subgrid-scale (SGS) velocity, i.e., the residual liquid fluctuations at the bubble position, was assessed by comparing cases 0 and 1. A series of snapshots of the evolving bubble plume colorized by magnitude of bubble's slip velocity and liquid fluctuations at its position for case 0 are shown in Figs. 2(a)–(d) and 11(a)–(d), respectively. The bubble's slip velocity varies only within a small range throughout the column (mostly between 0.2 and 0.35 m/s). The magnitude of the liquid fluctuations at bubbles' position, which is approximately one order of magnitude lower than the slip velocity, varies throughout the column and decreases from the bottom towards the top of the column.

It can be seen in Fig. 12(a) that the predicted average liquid velocity with and without the incorporation of the SGS velocity are quantitatively different. The position of the local maximum was shifted away from the center of the column with a lower velocity magnitude (about 0.02 m/s) than that predicted by the case 0. It might be that, without the SGS velocity, the fluctuation of the plume cannot be correctly predicted. In Fig. 12(b) and (c), the vertical and the lateral component of the resolved fluctuating

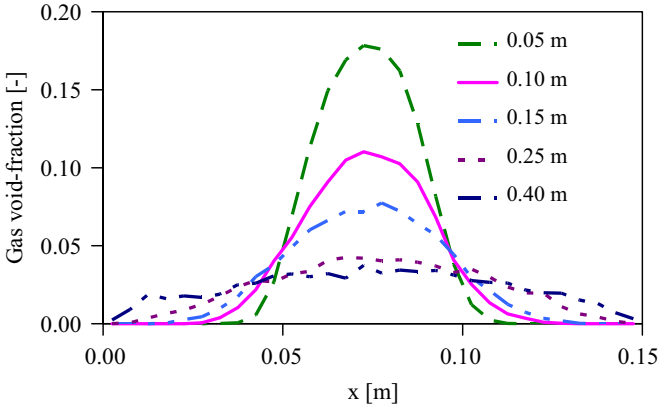

Fig. 10. Long-term average of the gas void-fraction at various height levels in the mid-depth plane.

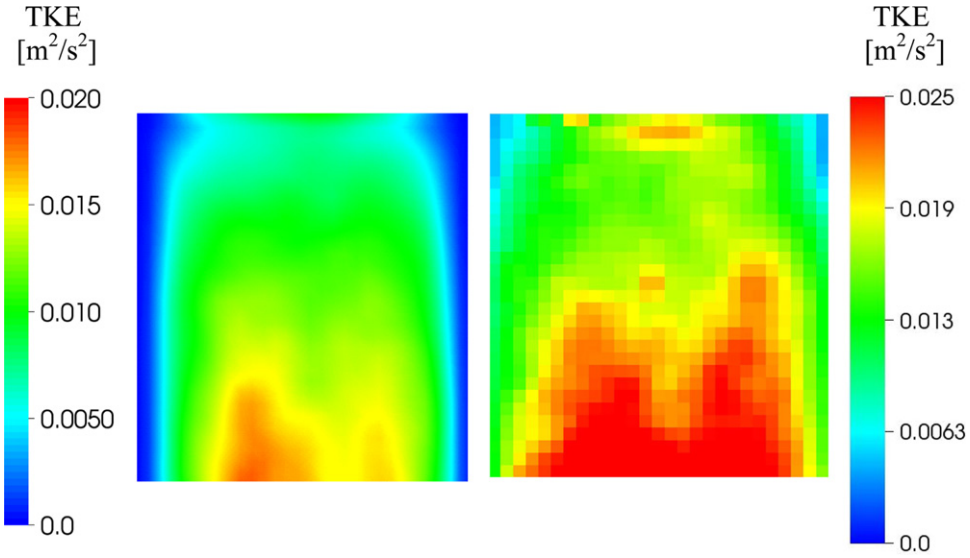

Fig. 9. Predicted and experimental long-term average of the turbulent kinetic energy in the mid-depth plane at the upper part of the bubble column. Note that different color scales are used. (For interpretation of the references to color in this figure legend, the reader is referred to the web version of this article.)

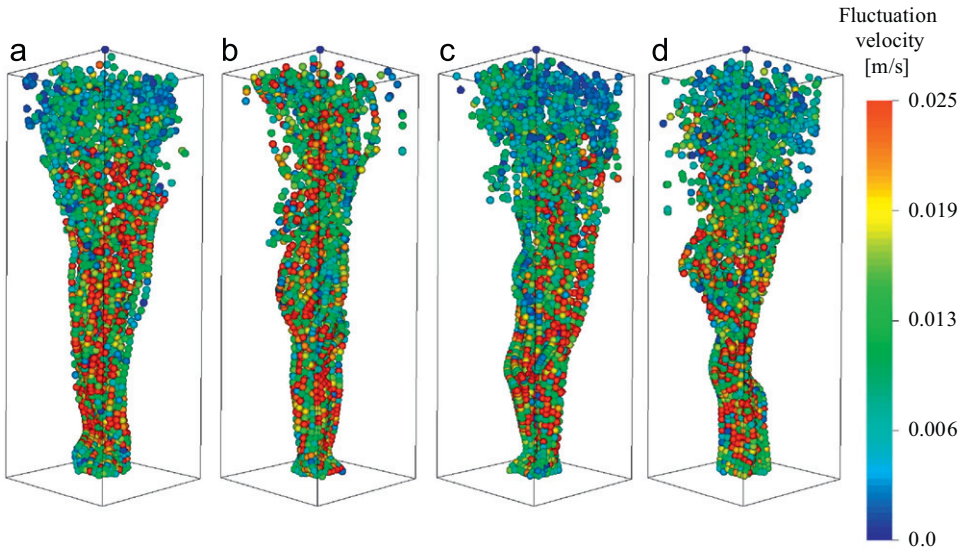

Fig. 11. Snapshots of the bubble dispersion pattern after 20, 50, 100 and 150 s. The bubbles are colored by the magnitude of the liquid fluctuations at its position. Note that the bubbles are magnified for visualization purpose, not to scale. (For interpretation of the references to color in this figure legend, the reader is referred to the web version of this article.)

liquid velocity obtained from the cases 0 and 1 are shown. Similar qualitative and quantitative deviations can be observed in the resolved fluctuating components. These results point out that the inclusion of the SGS velocity has some effect on the dispersion pattern of the bubbles, which can be seen in the predicted results. It can be anticipated that the inclusion of the SGS velocity is beneficial for an accurate prediction of the motion of the bubbles, and hence, the mean velocity profile. In denser systems with significantly stronger bubble–bubble interactions, a significant improvement should be obtained. It is important to note that the stochastic inter-particle collision model also produces fluctuations due to its stochastic nature. Therefore, larger differences between the simulations with and without SGS velocity might be obtained when the direct collision model for bubbles is used.

3.3. Effect of the Smagorinsky constant C_S

In the present study, the turbulence generated by bubbles, i.e., the so-called "bubble-induced turbulence", is not specifically modeled. Hence, the impact of the Smagorinsky constant C_S was studied by varying its value. The analysis is carried out based on the case with C_S=0.10 (i.e., case 0) in comparison to a lower C_S=0.08 (case 2) and a higher C_S=0.12 (case 3). Fig. 13(a)–(c) shows the comparison between the experimental and predicted profiles of the mean vertical velocity and fluctuating velocity components of the liquid phase. It can be seen that in the case with higher C_S, the predicted mean profile is almost equal to the case of C_S=0.10, while a lower C_S provides the least good agreement between experiment and simulation. This is due to the fact that with a decrease of C_S, the turbulent viscosity is also decreased. Consequently, the fluctuations of the bubble plume get stronger, resulting in a higher collision frequency and lower average velocity profiles. This phenomenon only slightly influences the flow field in the case with higher C_S. It can also be seen that, both vertical and lateral fluctuating components are affected by the choice of C_S in the similar manner. We conclude that the variation of C_S has only marginal effect to the predicted flow fields and an improvement can be made only by incorporating a reliable multiphase turbulence model.

3.4. Sensitivity of the grid size ratio to the bubble diameter

As discuss earlier, the grid size ratio to the bubble diameter h/d_p should compromise between a sufficiently fine grid resolution to capture the most energetic eddies and a sufficiently coarse grid resolution to stay close to the Millelli criterion. Here we studied the influence of h/d_p by carrying out simulations with a h/d_p value equal to 1.25 (the standard case, case 0), 1.50 (case 4) and 1.10 (case 5). Fig. 14(a)–(c) shows the comparison of the predicted profiles of the mean vertical velocity and fluctuating velocity components of the liquid phase with various h/d_p. As expected, the simulation with the highest h/d_p value, i.e., the coarsest grid size, provides large deviations from the experimental data. Although the h/d_p value is closest to the Millelli criterion, the grid size is too coarse for resolving the flow field and correctly coupling between phases. Decreasing the h/d_p value from 1.25 to 1.10 slightly improves the prediction at the expense of computational resources. Therefore, we concluded that, in this work, the h/d_p value of 1.25 provides a satisfactory level of accuracy along with reasonable computational expenses and the refinement of the h/d_p value to 1.1 does not deteriorate the prediction.

3.5. Speedup and scalability on parallel platforms

In order to analyze the parallelization performance of the presented modeling technique, the concepts of speedup and scalability are employed. The speedup concept represents the relative reduction of execution time when a parallel execution on p processors is performed. According to Rauber and Rünger (2009), the speedup $S_p(n)$ of a parallel program with n processors with a parallel execution time $T_p(n)$ is defined as

$$S_p(n) = \frac{T_p(1)}{T_p(n)}, \tag{12}$$

with $T_p(1)$ being the execution time to solve the same problem using the sequential version of the parallel implementation.

The scalability of a parallel program expresses the efficiency of the program while increasing the problem size with a fixed number of n processors. The scalability $S_s(m)$ is defined here as a proportion of the execution time $T_s(m)$ of a problem with a size m to the execution time of a problem with an appropriate selected

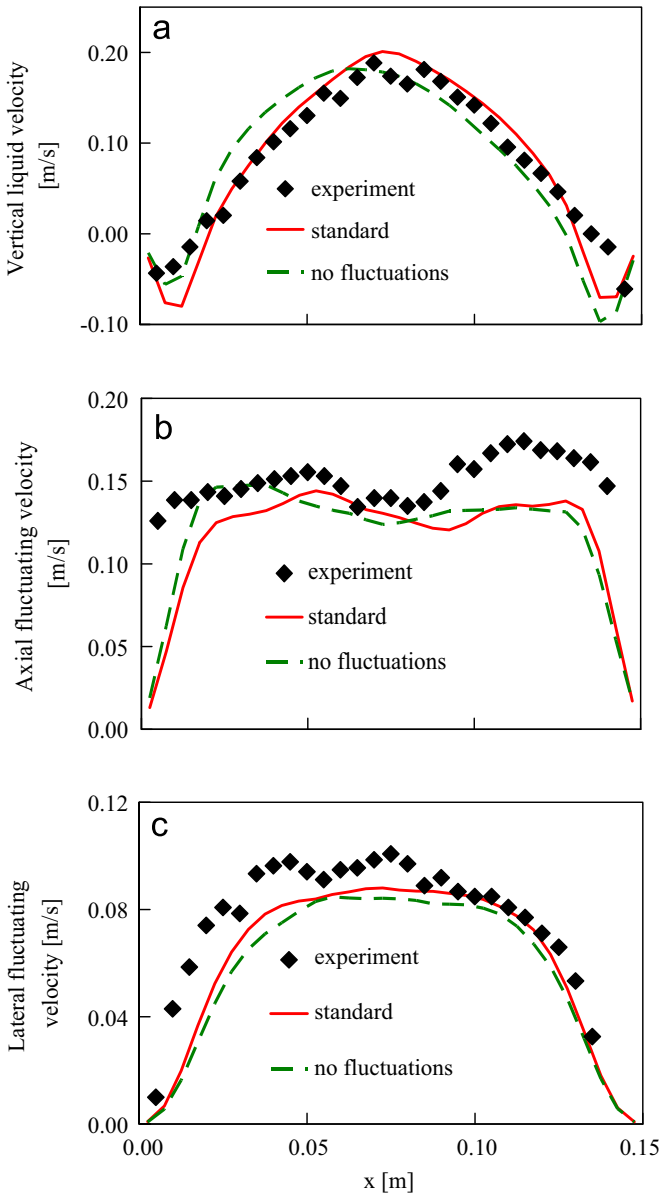

Fig. 12. Comparison of the predicted and experimental average liquid velocity and the fluctuating velocity components for the standard case (case 0) and the case without subgrid-scale fluctuations (case 1) at a height of 0.28 m and a depth of 0.075 m.

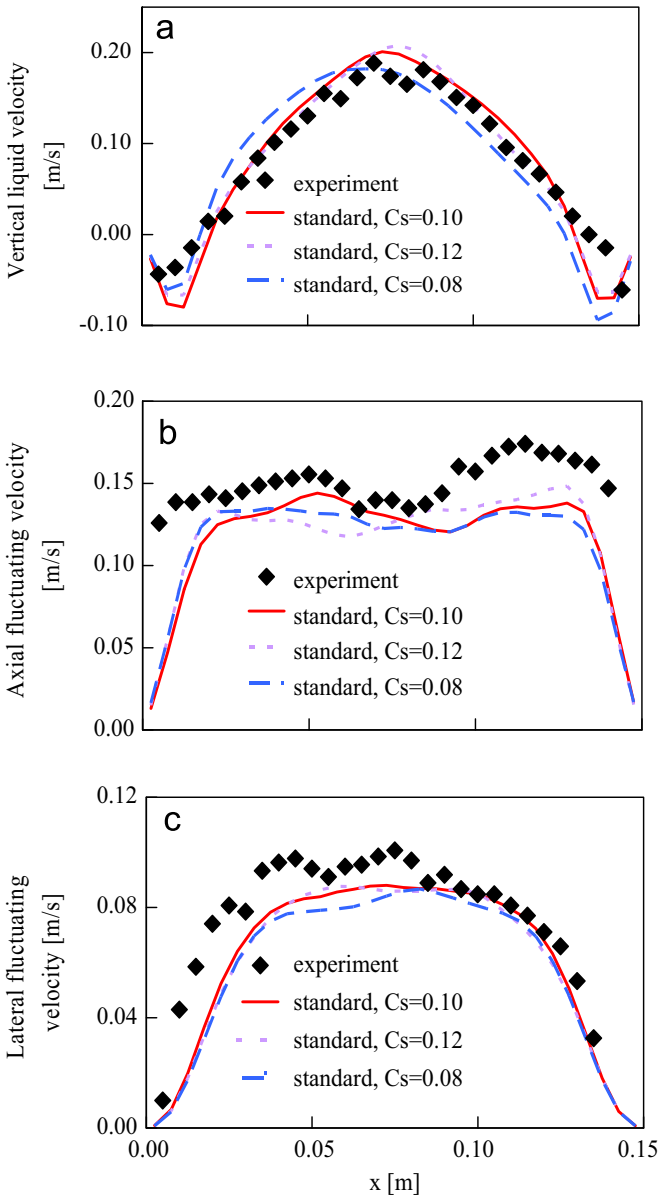

Fig. 13. Comparison of the predicted and experimental average liquid velocity and fluctuating velocity components for the standard case (case 0) with various values of the Smagorinsky constant (case 2 and 3) at a height of 0.28 m and a depth of 0.075 m.

reference problem size $T_s(m_0)$

$$S_s(n) = \frac{T_s(m)}{T_s(m_0)}. \tag{13}$$

In the present paper, a simulation case with a computational domain of $640 \times 32 \times 32$ grid nodes was used to measure the speedup and scalability of the program using Sun X2100, dual core Opteron CPUs with Gigabit Ethernet. The settings are similar to the case 0 in the previous section, except that the bubbles are homogeneously generated throughout the computational domain to equally distribute the computational load at every processor. The studies were carried out for 1 s, i.e., 10,000 time steps.

Fig. 15(a) shows the speedup obtained with 1, 2, 4, 8, 16 and 32 processors. The simulation cases contain 64,000 bubbles in total at every instance. The measurement of the execution time for the dispersed gas phase and the continuous liquid phase are performed separately. The total speedup is the weighted average of the underlying dispersed and continuous phase calculation. It should be noted that in our cases, the computational time of the dispersed phase is approximately 85% of the total computational time. As can be seen, excellent overall and dispersed-phase speedups are obtained, while the speedup of the liquid phase decreases with an increasing number of processors. The reason for the deterioration of the speedup of the continuous phase part (i.e., the LB scheme calculation) in our test case is that the layers being calculated on each processor are the sum of the real domain layers and the ghost layers (including the communication of these layers). Therefore, the computational resources being used for the ghost layer become significant when the number of processors increases. For instance, based on our test case, with 16 processors each processor performs a calculation of 40 real domain layers and 6 ghost layers, i.e., the ratio is 40:6, while the ratio is equal to 20:6 with 32 processors. Thus, the calculation of the ghost layers is increased from 15% to 30% of the total LB scheme calculation. An alternative might be to perform two-dimensional parallelization. It is important to emphasis again that the overall

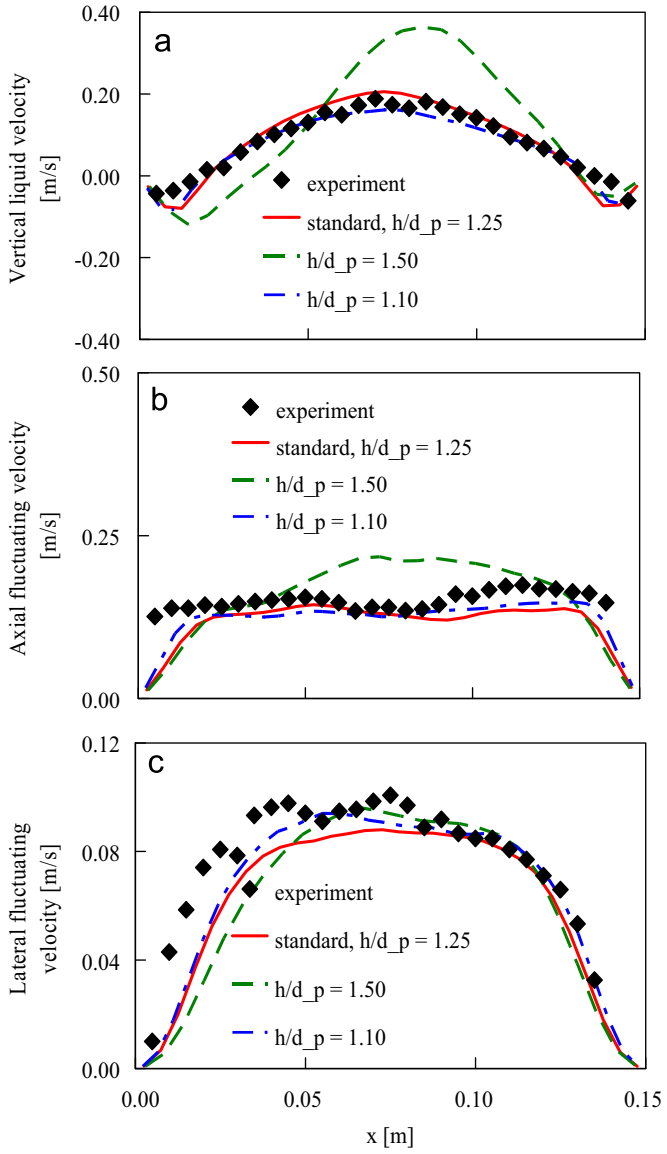

Fig. 14. Comparison of the predicted and experimental average liquid velocity and fluctuating velocity components for the standard case (case 0) with various grid size ratio to the bubble diameter (h/d_p) (cases 4 and 5) at a height of 0.28 m and a depth of 0.075 m.

performance is dominated by the Lagrangian particle tracking part, which takes approximately 85% of the calculation time. Therefore, the main benefit from the presented modeling technique is the high parallel efficiency of the stochastic Lagrangian particle tracking, the well-known flexibility of complex geometry handling provided by the LB scheme, and the parallel performance of the LB scheme (when an appropriate ratio between the real domain layers and the ghost layers is used). This provides an alternative for simulations of multiphase dispersed flow within large-scale and complex geometries, e.g., flows in a multiphase stirred vessel. It is also important to note that, although an excellent overall speedup has been obtained, the time step used in this study is approximately two orders of magnitude smaller than the conventional CFD calculation, e.g., in the work of Zhang et al. (2006). Therefore, the maximum benefit of using a LB-based simulation can be obtained when solving a large-scale problem where a massive parallelization can be utilized.

The scalability of the program is shown in Fig. 15(b). In this comparison, the base case has a total number of 40,000 bubbles, while the number of bubbles is equal to 4,000,000 in the largest case. The computational domain is kept constant in every case. The execution time used in this analysis is only the execution time of the dispersed gas phase. An excellent scalability of the program is obtained. Fig. 15(b) shows that an increase of the problem size does not lead to an increase of the simulation time. For example, a 100-fold increase of the problem size leads to a 90-fold increase of the simulation time. This might be attributed to the fact that the Eulerian part of the dispersed phase calculation is kept constant, independent to the number of bubbles, while the scalability of the Lagrangian part is linear.

4. Conclusions

A novel modeling technique for the simulation of turbulent gas–liquid bubbly flows according to the Eulerian–Lagrangian (EL) approach has been presented. Each individual bubble was treated as a single, point-volume particle and was tracked in a turbulent liquid flow field. The turbulence in the liquid phase was represented by filtered conservation equations. The impact of the residual (sub-filter) fluctuation components on the motion at the grid scales was modeled using the Smagorinsky model. It was shown that the choice of the Smagorinsky constant C_S slightly affects the predicted flow field with the best result obtained using $C_S = 0.10 - 0.12$. It is important to note that the filtering process

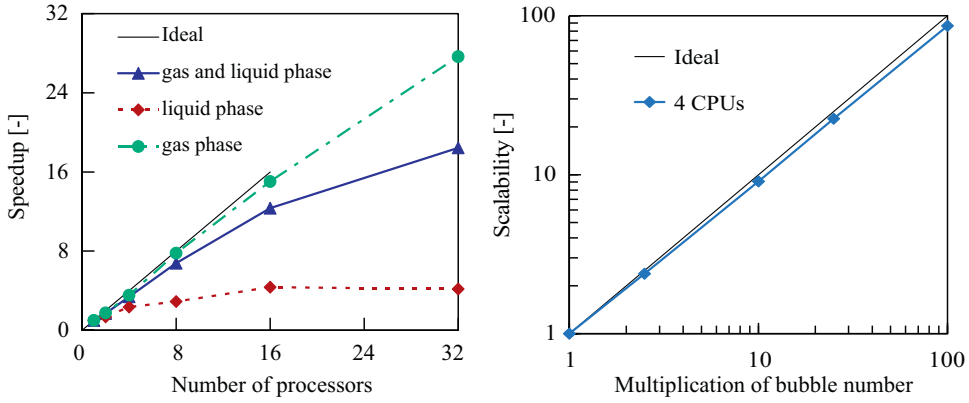

Fig. 15. Speedup and scalability of the present modeling technique. The simulations were performed for $640 \times 32 \times 32$ grid nodes and 64,000 bubbles. The simulations in the scalability study were performed using 4 processors and contain $640 \times 64 \times 64$ grid nodes with 40,000 bubbles in the base case (with a multiplication factor of 1) and 4,000,000 bubbles in the largest case (with a multiplication factor of 100).

employed here should be viewed as an engineering model, rather than a large eddy simulation (LES). This is due to the restriction of our EL approach that requires the grid size should be larger than the bubble size. Consequently, the grid space is too coarse to sufficiently resolve the flow field required for a regular LES. The motion of bubbles was computed considering gravity/buoyancy, fluid stresses, drag, lift and added mass forces. The Basset history force was neglected for physical (and computational) reasons. It is well known that as of yet there is no universal inter-phase closure model available for the simulation of bubbly flow. Thus, a set of appropriate empirical correlations for the inter-phase closures was carefully chosen from the literature.

Specifically the main results of this work are:

- It has been demonstrated that due to the coarse grid space used in the simulations, the residual fluctuating velocity components of the liquid phase have a significant effect on the bubbles motion, which is represented by the predicted mean and fluctuating flow fields. In our work, the residual fluctuations were considered by means of a Langevin equation model.
- Collisions between bubbles were considered using a stochastic inter-particle collision model. The model is based on the generation of a fictitious collision partner and a collision probability according to the kinetic theory. The collision model dramatically decreases computing time compared to the direct collision method and provides excellent computational efficiency on parallel platforms.
- The predicted results were compared with experiments of Deen et al. (2001). Both mean and fluctuating velocities are in excellent quantitative and qualitative agreement with the measured data. Furthermore, the subgrid model used (i.e., the Smagorinski model) provides an excellent agreement between experimental and simulation data. Thus, the simulation can be used to obtain detailed, quantitative insight into the dynamics of the dispersed and the continuous phase in the bubble column.
- The speedup and the scalability of the presented modeling technique on parallel platforms have been analyzed. Excellent overall parallelization performance and scalability of the program were demonstrated. The maximum benefit of the presented modeling technique can be obtained when a large-scale simulation, in which the characteristic length is several order larger than the bubble diameter, and a massive parallelization are realized.

While the study presented here has been carried out for a bubble column with a relatively low global gas holdup (approximately 1%), the modeling techniques can be applied to a wide range of problems, involving turbulent gas–liquid bubbly flow in stirred systems. Nevertheless, in order to deal with real industrial problems, which often involve a high global gas holdup, further work will address for the inclusion of the gas void fraction in the conservation equations, the void fraction dependence of drag force, as well as models for bubble coalescence and breakup.

Acknowledgment

The authors wish to thank the reviewer for providing the experimental data of the Deen case.

Appendix

Correlation function in Langevin equation model

$$R_p(\Delta t,\Delta r) = R_L(\Delta t) \times R_E(\Delta r). \tag{A1}$$

The Lagrangian velocity auto-correlation function

$$R_L(\Delta t) = \exp\left(-\frac{\Delta t}{T_L}\right). \tag{A2}$$

The Lagrangian integral time scale

$$T_L = c_T \frac{\sigma_{SGS}^2}{\varepsilon} \text{ with } c_T = 0.4. \tag{A3}$$

The Eulerian correlation tensor

$$R_{E,ij}(\Delta r) = \{f(\Delta r) - g(\Delta r)\}\frac{r_i r_j}{r^2} + g(\Delta r)\delta_{ij}, \tag{A4}$$

with

$$f(\Delta r)_i = \exp\left(-\frac{\Delta r}{L_{E,i}}\right), \quad g(\Delta r)_i = \left(1-\frac{\Delta r}{2L_{E,i}}\right)\exp\left(-\frac{\Delta r}{L_{E,i}}\right). \tag{A5}$$

The integral length scale

$$L_{E,x} = 1.1 T_L \sigma_{SGS}, \quad L_{E,y} = L_{E,z} = 0.5 L_{E,x}. \tag{A6}$$

The particle response time

$$\tau_p = \frac{4}{3}\frac{d_p^2}{C_D|\mathbf{u}-\mathbf{u}_p|} \text{ where } Re > 1. \tag{A7}$$

References

Bernaschi, M., Fatica, M., Melchionna, S., Succi, S., Kaxiras, E., 2010. A flexible high-performance lattice Boltzmann GPU code for the simulations of fluid flows in complex geometries. Concurrency and Computation: Practice and Experience 22l, 1–14.

Deen, N.G., 2001. An experimental and computational study of fluid dynamics in gas–liquid chemical reactors. Ph.D. Thesis. Aalborg University Esbjerg. Denmark.

Deen, N.G., Solberg, T., Hjertager, B.H., 2001. Large eddy simulation of the gas–liquid flow in a square cross-sectioned bubble column. Chemical Engineering Science 56, 6341–6349.

Deen, N.G., Van Sint Annaland, M., Kuipers, J.A.M., 2004. Multi-scale modeling of dispersed gas–liquid two-phase flow. Chemical Engineering Science 59, 1853–1861.

Delnoij, E., 2001. Fluid dynamics of gas–liquid bubble columns: a theoretical and experimental study. Ph.D. Thesis. Twente University. The Netherlands.

Derksen, J.J., 2003. Numerical simulation of solids suspension in a stirred tank. AIChE Journal 49, 2700–2714.

Derksen, J.J., 2010. Simulations of lateral mixing in cross-channel flow. Computers and Fluids 39, 1058–1069.

Derksen, J.J., Van den Akker, H.E.A., 1999. Large eddy simulations on the flow driven by a Rushton turbine. AIChE Journal 45, 209–221.

Derksen, J.J., Van den Akker, H.E.A., Sundaresan, S., 2008. Two-way coupled large-eddy simulations of the gas–solid flow in cyclone separators. AIChE Journal 54, 872–885.

Eggels, J.G.M., Somers, J.A., 1995. Numerical simulation of free convective flow using the lattice-Boltzmann scheme. International Journal of Heat and Fluid Flow 16, 357–364.

Hirt, C.W., Nichols, B.D., 1981. Volume of fluid (VOF) method for the dynamics of free boundaries. Journal of Computational Physics 39, 201.

Ho, C.A., 2004. Modellierung der Partikelagglomeration im Rahmen des Euler/Lagrange–Verfahrens und Anwendung zur Berechnung der Staubabscheidung im Zyklon. Ph.D. Thesis. Martin-Luther-Universität Halle-Wittenberg. Germany.

Hu, G., 2005. Towards large eddy simulation of dispersed gas–liquid two-phase turbulent flows. Ph.D. Thesis. West Virginia University. United States.

Hu, G., Celik, I., 2008. Eulerian–Lagrangian based large-eddy simulation of a partially aerated flat bubble column. Chemical Engineering Science 63, 253–271.

Joshi, J.B., 2001. Computational flow modeling and design of bubble column reactors. Chemical Engineering Science 56, 5893–5933.

Loth, E., 2000. Numerical approaches for motion of dispersed particles, droplets and bubbles. Progress in Energy and Combustion Science 26, 161–223.

Milelli, M., Smith, B.L., Lakehal, D., 2001. Large-eddy simulation of turbulent shear flows laden with bubbles. In: Geurts, B.J., Friedrich, R., Metais, O. (Eds.), Direct and Large-Eddy Simulation-IV. Kluwer Academic Publishers, Dordrecht, The Netherlands, pp. 46–470 vol. 8 of ERCOFTAC Series.

Nicěno, B., Boucker, M., Smith, B.L., 2009. Euler–Euler large eddy simulation of a square cross-sectional bubble column using the Neptune CFD code. Science and Technology of Nuclear Installations Article 410272.

Pozorski, J., Apte, S.V., 2009. Filtered particle tracking in isotropic turbulence and stochastic modeling of subgrid-scale dispersion. International Journal of Multiphase Flow 35, 118–128.

Press, W., Teukolsky, S., Vetterling, W., Flannery, B., 1986–1992. Numerical Recipe in Fortran 77 second ed. Cambridge University Press.

Ranade, V.V., 2002. Computational Flow Modeling for Chemical Reactor Engineering. Academic Press.

Rauber, T., Rünger, G., 2009. Parallel Programming for Multicore and Cluster Systems. Springer.

Smagorinsky, J., 1963. General circulation experiments with the primitive equations: 1. The basic experiment. Monthly Weather Review 91, 99.

Somers, J.A., 1993. Direct simulation of fluid flow with cellular automata and the lattice-Boltzmann equation. Journal of Applied Sciences Research 51, 127–133.

Sommerfeld, M., 2001. Validation of a stochastic Lagrangian modeling approach for inter-particle collisions in homogeneous isotropic turbulence. International Journal of Multiphase Flow 27, 1829–1858.

Sommerfeld, M., Bourloutski, E., Broeder, D., 2003. Euler/Lagrange calculations of bubbly flows with consideration of bubble coalescence. The Canadian Journal of Chemical Engineering 81, 508–518.

Sommerfeld, M., Kohnen, G., Rueger, M., 1993. Some open questions and inconsistencies of Lagrangian particle dispersion models. In: Proceedings of the Ninth Symposium on Turbulent Shear Flows. Kyoto. Japan. Paper No. 15-1.

Unverdi, S.O., Tryggvason, G., 1992. A front-tracking method for viscous, incompressible multi-fluid flow. Journal of Computational Physics 100, 25–37.

Van den Hengel, E.I.V., Deen, N.G., Kuipers, J.A.M., 2005. Application of coalescence and breakup models in a discrete bubble model for bubble columns. Industrial and Engineering Chemistry Research 44, 5233–5245.

Zhang, D., Deen, N.G., Kuipers, J.A.M., 2006. Numerical simulation of the dynamic flow behavior in a bubble column: a study of closures for turbulence and interface forces. Chemical Engineering Science 61, 7593–7608.